PACS numbers: 68.55.Ln, 81.15.Cd

ENHANCEMENT OF NMP DEGRADATION UNDER UV LIGHT BY NITROGEN-DOPED TiO$_2$ THIN FILMS USING A DESIGN OF EXPERIMENT

H. Fakhouri[1], W. Smith[1], J. Pulpytel[1], A. Zolfaghari[2], H. Mortaheb[2], F. Meshkini[2], R. Jafari[2], F. Arefi-Khonsari[1]

[1] Laboratoire de Genie des Procedes Plasmas et Traitements de Surfaces (LGPPTS), Universite Pierre et Marie Curie (UPMC),
ENSCP, 11, Rue Pierre et Marie Curie, 75231, Paris, Cedex 05, France
E-mail: jerome-pulpytel@enscp.fr

[2] Chemistry and Chemical Engineering Research Center of Iran,
Tehran, Iran

Doping nitrogen within TiO$_2$ is an effective way to enhance visible light photocatalysis due to a direct electron excitation from the N$_{2p}$ states within the band gap. However, nitrogen doping is not always efficient for UV photocatalytic activity. Here, different structures of N-doped TiO$_2$ (TiO$_x$N$_y$) have been prepared by reactive RF (13.56 MHz) magnetron sputtering. The morphological, optical, structural, and photocatalytic properties of the films have been studied in order to investigate the competitive effect of the morphology and the chemical composition on the efficiency of the photocatalytic activity. The variation of surface wettability of the film over time in the dark and under visible and UV irradiation was also studied. The reduction in wettability by dark storage can be explained by the adsorption of hydrocarbon contamination on the thin film's surface. Additionally, from water contact angle experiments, it was found that these films developed hydrophilic properties upon UV and visible illumination. The photoinduced change in the contact angle of water was due to the removal of hydrocarbon contamination on the surface and also the photo-oxidation of the water droplet. Samples prepared at high pressure gave the best photocatalytic activity, even though the deposition rate was lower at higher pressures (lower film thicknesses), due to the high specific surface area and the optimal presence of TiO$_x$N$_y$ crystals in the lattice. However, at low pressure, the TiN crystals became more predominant, and acted as recombination centers for the photo-generated charge carriers. A design of experiments was used in order to optimize the deposition parameters to have the best photocatalytic activity. The high photocatalytic activity under UV light was found to be due to the introduction of discrete energy levels within the band gap, the increased sample wettability, and the higher specific surface area. However, the post annealing process did not effect the activity under UV irradiation. Using the response surface methodology, RSM, based on a design of experiment, DOE, we are able to achieve a good understanding of the complex processes involved in the deposition of the thin films and their effect on the photocatalytic activity.

Keywords: TIO$_2$ THIN FILM, DOE, RSM (RESPONSE SURFACE METHOD), NMP, PHOTOCATALYSIS, NITROGEN DOPING, SPUTTERING.

(Received 04 February 2011)

1. INTRODUCTION

TiO_2 has shown tremendous applications as an effective photocatalyst under UV light irradiation [1-7]. It is a readily available material that is low cost, has good thermal and aqueous stability and resistivity, and is adverse to corrosion and photocorrosion. TiO_2 has shown the ability to photodegrade many organic pollutants dissolved in water via UV irradiation.   Among organic pollutants, N-methyl-2-pyrrolidone, (NMP), is one of the most common found in the wastewater of many factories due to its common and cast usage. NMP is an important, versatile solvent and reaction medium for the chemical industry such as petrochemical, plastics, coating, agricultural, and electronics, because of its low volatility, thermal stability, high polarity and aprotic, noncorrosive properties [8]. However, due to its large band gap TiO_2 absorbs visible light poorly, and thus has been an ineffective visible-light photocatalyst. Many attempts have been made to improve the photocatalytic activity of TiO_2 under UV and/or visible light irradiation. In particular, the focus has been on decreasing the band gap energy of TiO_2 (about 3.2 eV), such that it is suitable to absorb visible light, i.e. 1.6 - 3.0 eV, particularly at 2.5 eV, which corresponds to the solar maximum output. The efforts to modify the optical properties of TiO_2 have been attempted by three primary methods; (1) doping TiO_2 with transition metal ions (Cr, V, Mn, etc.) in order to produce intermediate states in the band-gap close to the conduction band [9-13], or/and with anionic dopants (F,C, N, ...) close to the valence band [14-17]. (2) sensitization by attaching photo-sensitizers such as organic substances, semiconductors, and metal halides that are able to absorb visible light [18-20], and (3) the formation of reduced TiO_2 containing oxygen vacancies [21-23], including reduction with hydrogen [24]. While there are a plethora of available doping methods, some processes can hurt the overall photoactivity of the TiO_2 samples. For instance, some doping methods suffer from thermal or photoactivite instability, an increase in the recombination between the photogenerated electron-hole pairs, and the poor reproducibility of the photocatalytic activity [25-26].

In particular, Asahi et al. [27] initially set three requirements to achieve visible-light photoactivity for TiO_2: (i) doping should produce states within the band gap of TiO_2 that absorb visible light; (ii) the conduction band CB minimum and the dopant states must be above the H_2/H_2O reduction level to ensure photoreductive activity; and (iii) sufficient overlap between the intergap and band states of the photocatalyst in order to provide a fast transfer of photoexcited carriers to the reactive states at the surface within their lifetime. Metal dopants do not meet conditions (ii) and (iii) as they produce localized d-states deep within the band gap of TiO_2 and tend to act more as electron-hole pair recombination centers. In practice, metal doping has shown both positive and negative effects on the photocatalytic activity of TiO_2, under both UV and visible light [28-29].

An important factor in the applicable photoactivity of doped-TiO_2 is based on the density of states (DOS) that make up the photoactive energy levels, i.e. the valence band, the conduction band, and the doped energy band level. The density of states determine the transition probability for photoexcitation from either the valence band or dopant energy level, to the conduction band level, which is governed by Fermi's Golden Rule. DOS calculations have been carried out using anionic dopants such as C, N, F, P [30] and S [31] (however, Sulfur doping is not commonly employed due to its large ionic radius even if it can narrow the band gap [31]). The most interesting results are that with carbon

[15] and nitrogen, which can generate intermediate impurity states above the maximum of the valance band within the band gap [16, 30, 32-34]. Interstitial and substitutional carbon doping may decrease the TiO_2 band gap to 2.32 eV which is even less than the known Rutile band gap (about 3.0 eV), so the photoinduced charge carriers can be generated more easily under visible light irradiation in C-doped TiO_2 [15]. However, the mobility of the photogenerated holes may be reduced, which will not improve the photooxidation activity which takes place via a cationic exchange, even if the measured photocurrent is increased anionically [28].

Nitrogen doped TiO_2 has received significant attention, and the results have yielded many contradictions. The DOS results (Asahi et al. for example) suggest that the substitutional nitrogen doping is more effective than interstitial doping (and the mixture of both substitution and interstitial) due to the introduction of localized N_{2p} states just above the valance band which can mix with O_{2p} states (N—O bonding), allowing the absorption of visible light up to 500 nm. Sangwook Lee et al [35] found that interstitial N doping creates defects at levels deep within the band gap which disturb the charge transfer in the TiO_2 nanoparticles. However, other works found that interstitial N-doping is more effective than substitutional doping [35-36]. Diwald et al. [37-38] found that interstitial doping shows more photoactivity due to the suppressing photo-threshold in opposition of substitutional dopants. Other results have shown that a multi-type N doping (interstitial *and* substitutional) gives very good photocatalytic activity in visible light [39].

Although some of the past literature has found discrepancies in the nature and function of nitrogen doping, there are a few common themes that have become evident. While doping TiO_2 with nitrogen can decrease the band gap, and thus allow an improvement in visible light absorption, the nitrogen band energies that allow this absorption also can act as recombination centers that decrease the lifetime of photogenerated charge carriers, which decrease the overall photocatalytic efficiency. There exists a delicate balance in the concentration (and nature) of N-doping in TiO_2 that must be achieved in order to maximize the visible light absorption, while minimizing the electron-hole recombination. The purpose of this study is to find the sputtering deposition parameters that allow for the optimal optical and photocatlytic properties of N-doped TiO_2 films.

Sputtering deposition is one of the most promising techniques for uniform coatings over a large area as it has the advantage of producing a well controlled film in terms of morphology, crystallinity and stochiometry. The reactive RF magnetron sputtering of TiO_2 is of great importance because it has shown the ability to prevent target poisoning [40-45], and it also permits desirable and reproducible properties of the deposited films with good deposition rate at different substrate temperatures, as well as a good homogeneity of thickness and composition of films on a large scale with a flat surface. In addition, reactive RF magnetron sputtering of titanium dioxide has a high degree of flexibility to control the structural and physical properties of the films by varying several process parameters such as the sputtering pressure, sputtering power, target to substrate distance, reactive gas partial pressure, substrate temperature and using DC and RF substrate biasing [42, 44, 46-49].

The study of the individual processing parameters affecting photocatalytic activity is quite complicated due to the abundance of physical, chemical, and electronic procedures that take place, as well as the abundance of sputtering

controls, detailed above. The use of response surface methodology, RSM, based on design of experiment is one way to simplify complex processes since it allows multiple physical characteristics to be compared simultaneously. The resolution of the empirical polynomial equation that determines the RSM can be used to understand and predict the optimization of the photocatalytic activity of N-doped TiO_2 by comparing the material properties with the process parameters and functional activity. In this work, we used a design of experiment to investigate the morphological, structural, and optical properties of N-doped TiO_2 thin films with various nitrogen concentrations, and how they affect the UV light photocatalysis of NMP.

2. EXPERIMENTAL

2.1 Thin films preparation

The un-doped and N-doped TiO_2 thin films were prepared by a RF reactive magnetron sputtering system. A metallic Ti target (50 mm diameter) having a purity of 99.95%, was sputtered in a reactive gas atmosphere containing Ar, O_2 and N_2. Different nitrogen to oxygen ratios were used, ranging from 0 to 14 %, while the argon flow rate was fixed to 30 sccm. The substrates used were electro-polished stainless steel, Si (100) wafers and ordinary microscope glass slides. Prior to deposition, the non metallic substrates were ultrasonically cleaned with acetone, ethyl alcohol and then de-ionized water for 20 minutes each. The RF cathode power was 200 W for all the depositions in order to minimize the target poisoning effect [41-42] since titania is a semi-conducting oxide, and can easily contaminate the target. Using optical emission spectroscopy (OES), we followed the Ti emission lines at 517 and 521 nm, and controlled the TiO_2 deposition parameters in order to have a fixed intensity of the Ti peaks during the deposition period. We stabilized the deposition rate in the intermediate region between two stable sputtering modes, reactive and metallic. The substrate holder was maintained at 300°C. The distance between the substrate holder and the target was fixed at 100 mm. The initial base pressure was between 3 to 7×10^{-6} torr, while the total working pressure was between 3 to 14 mtorr. Prior to each deposition, the target was pre-sputtered in Argon atmosphere for 10 minutes to remove any contaminations from the target surface. The film thicknesses were measured, and ranged from 80 to 500 nm. Some of the films were annealed for 1 hour at 450 °C in air atmosphere. The TiO_xN_y films in this paper were labeled as following: Pr for pressure, and N for the ratio of the nitrogen to oxygen flow rates.

2.2 Contact angle measurement

Contact angle measurements were performed by measuring the angles at which the liquid/vapor interface from a 6 µl water droplet meets the liquid/solid sample surface. Initial tests were performed for each sample under no light irradiation and the contact angle variation was studied over the course of two months. Further tests were conducted for different intervals of illumination with the full spectra of a Halogen and UV lamps. The time needed for a drop of water to return to the initial contact angle (of the fresh sample) after 2 months of dark storage was measured. A set of three 6 µl droplets were used for each surface, and the average contact angle over time was measured and averaged.

2.3 Film structure and morphology

The crystal structure of thin films was characterized by X-ray diffraction (XRD) (X'Pert Pro PW3040-Pro, Panalytical Inc.) using Cu K-R radiation in Bragg-Brentano (θ-2θ) configuration. The average crystallite size was determined by means of standard θ-2θ XRD scans using the Scherrer Formula. X'Pert High Score pattern processing was used to collect and process the data. The Raman spectra were recorded in a backscattering geometry using a Renishaw InVia Raman-microscope system and the 633 nm excitation wavelength of a red laser, focused on a spot size of the order of 3 μm. Film morphology and thickness were measured by SEM-FEG.

2.4 Photocatalytic activity

N-methyl-2-pyrrolidone (NMP) was oxidized in the presence of the prepared thin films using an 11W lamp (Philips TUV low pressure Hg lamp for near monochromatic output at 254 nm) which was placed at the center of the reactor shielded by a vertically immersed quartz jacket. All the experiments were performed at constant temperature. NMP was obtained from Merck with purity of > 99 %. The concentration of NMP and produced intermediates were monitored during the experiments using HPLC-UV (KNAUER, Chromgate 3.1) with isocratic elution (3 - 10 % acetonitrile, 97 - 90 % water, 1 ml/min) on a reversed-phase Nucleosil C_{18} column. The detection wavelength was 214 nm.

2.5 Design of experiment

In order to determine how the individual process and material parameters affect the photocatalytic activity of TiO_2 thin films, we used the Doehlert design with 2 factors (nitrogen flow rate and sputtering pressure). In order to achieve the desired set of data, we used 7 experiments focused around a central parameter value, including one in the center [51-52]. We estimated the optimized conditions by the Response Surface Methodology, RSM, based on a second order model.

3. RESULTS AND DISCUSSION

3.1 Contact angle measurement

Depending on the deposition parameters, the prepared samples displayed two types of contact angle shapes (within 2 months). Fig. 1a and b present an example of the contact angle variation related to two types of samples prepared at high pressure and low pressure. It is apparent that the contact angle increases with time with two principal slopes before reaching a stationary value. Fig. 1b shows the contact angle variation after different intervals of illumination with the full spectra of a Halogen and UV lamp up to return to the initial value of the contact angle (of the fresh sample).

We distinguished two groups (types) of contact angle trends according to the controlled pressure during the film deposition. Here we present only an example of samples prepared at high and low pressure respectively (Fig. 1a). At high pressure (more than 9 mtorr) the contact angle increases slowly and steadily up to a stable value about 10 % more than the initial contact angle value. However, samples prepared at low pressure show a different variation

following two mean slopes, a first order and a second order one up to a stable value up to 8 times over the initial contact angle value. Under visible irradiation, the wettability increases suddenly after a specific irradiation time which increases with increasing pressure up to reaching to the initial contact angle. The same conclusion can be seen under UV irradiation but the wettability is increased within a shorter time of UV irradiation and the surfaces become completely super hydrophilic regardless of the deposition pressure.
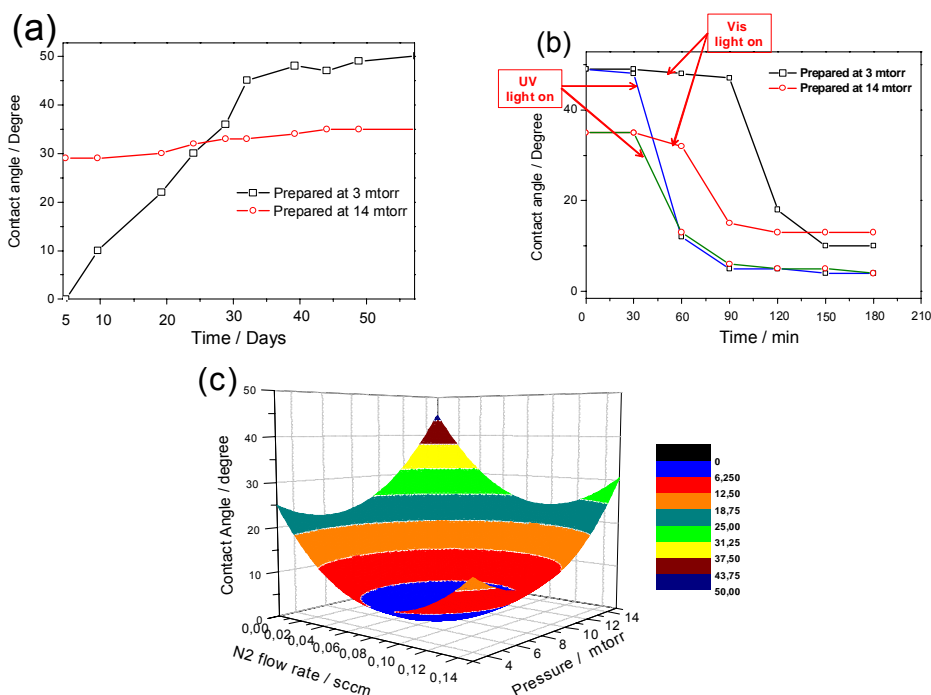
Fig. 1 – (a) The contact angle evolution during 2 months, being stored in the dark, (b) the change in contact angle under visible and UV light irradiation, and (c) the measured contact angle for different deposition pressures and nitrogen flow rates (the oxygen flow rate is fixed at 1.5 sccm, and contact angle is measured after 5 days of deposition)

The contact angle increased after storing the sample in the dark, possibly due to the adsorption of hydrocarbons on the photocatalyst surface. As the illumination exposure time is increased, the contact angle decreases from an initial value of ~50° (in the dark) to a final value of ~10є after two hours of illumination (the illumination period was in the absence of water droplet, and we used 6 μl de-ionized water droplet for each contact angle measurement on the same sample). These results are in agreement with literature [53], especially the model proposed by Wang et al. [50], which reported the photo induced change in contact angle of water to be due to the adsorption of hydrocarbon contamination on the surface of the thin film.

The contact angle enhancement, under irradiation, is due to two phenomena. First, under irradiation, the degradation of adsorbed hydrocarbons took place on the doped titania surface through the generation of OH radicals. Second,

illumination initiates the photo-oxidation of the water droplet, leading to a larger wettability of the surface. We used the wettability data, measured one week after the samples deposition, to modulate the response with two parameters, the pressure and the nitrogen flow rate. Fig. 1c presents the 3-D empirical iso-response curves, to identify the experimental region for minimum contact angle.

3.2 Impact of the sputtering pressure and film morphology

The microstructure of TiO_2 layers has a pronounced effect on the photocatalytic activity. The small pore size of the thin film allows only the top surface to be photocatalytically active. The sputtering process is able to grow column-like grain structures, and the spacing between columns can be controlled by the sputtering pressure [54]. The increased porosity increases the effective surface and active sites. For example, we can calculate the lateral ($S.A._{LAT}$) to geometrical ($S.A._{GEO}$) surface ratio for the film deposited at **14 mtorr** (Fig. 2a) which has the minimum thickness (**80 nm**),

$$\frac{S.A._{LAT}}{S.A._{GEO}} = \frac{4\pi D d}{\pi D^2} \tag{1}$$

where (*d*) is the film thickness and (*D*) is the column diameter. Using equation (**1**) and the morophological parameters measured by SEM, it is
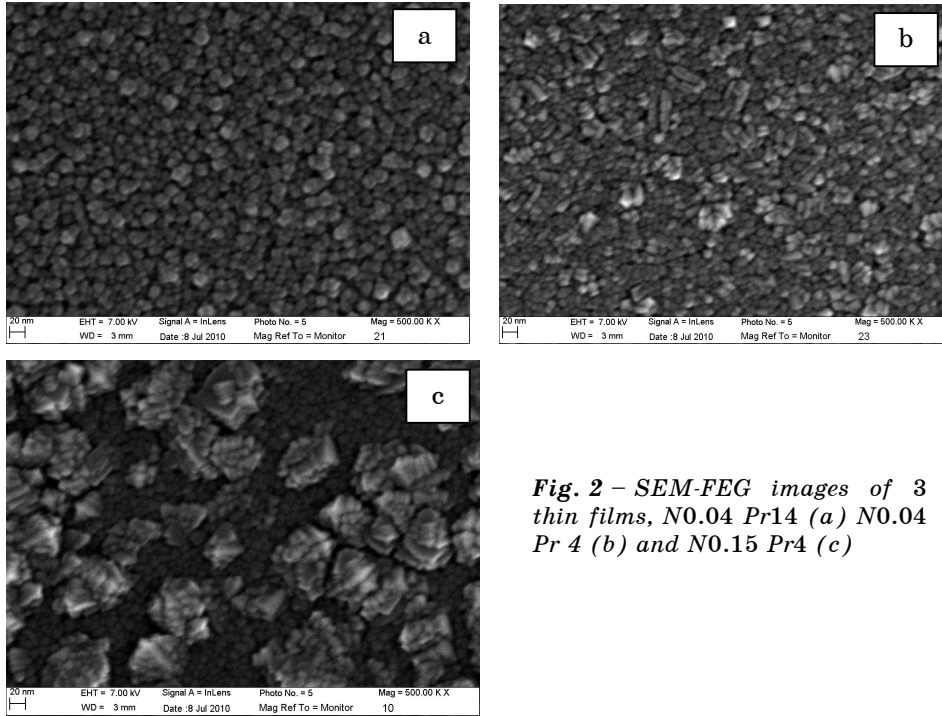
Fig. 2 – SEM-FEG images of 3 thin films, N0.04 Pr14 (a) N0.04 Pr 4 (b) and N0.15 Pr4 (c)

apparant that the available surface area is enhanced 10-fold when increasing the pressure from 4 to 14 mtorr, although it is important to note that the ratio is proportional to the film thickness.

As the TiO_2 crystals coalesce before reaching the substrate surface, their shape and size will stabilize. Normally, the crystal size increases up to a threshold that will further inhibit its growth. This maximum grain size is important for the inherent surface area of the thin film (the higher grain size would generate a higher porosity and a higher specific area) . The larger grain size would enhance the crystallinity which increases the adsorption of the pollutants, and thus show improved photodegradation. From Fig. 2 it is clear that at higher deposition pressure (comparing (a) with (b)), the film is more porous having a higher effective surface area. At a higher nitrogen flow rate (higher nitrogen concentration) it is possible to see the nucleation of TiO_xN_y clusters and this is more evident at high working pressure.

Fig. 3 shows the RMS for thickness in function of pressure and nitrogen flow rate. The thickness (and also the deposition rate) decreases sharply with the sputtering pressure. However, it is apparent that the nitrogen does not have any important impact on the deposition rate.
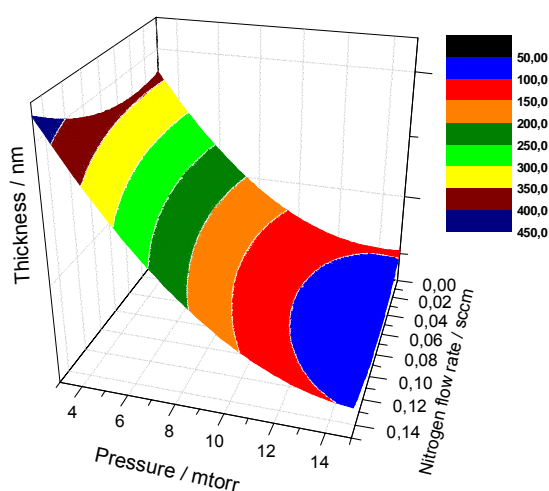
Fig. 3 − *Thickness of N doped TiO_2 thin films and iso-reponse curves (based on pressure and Nitrogen flow rate) from different samples data. Oxygen flow rate is fixed to be 1.5 sccm*

3.3 XRD analysis and Raman spectroscopy

The photocatalytic activity of TiO_2 depends on a variety of parameters including, but not limited to, the TiO_2 crystalline structure, crystal/particle size, surface morphology and the concentration/nature of the doping element. The crystalline phase of TiO_2 remains one of the principal factors that determines the photocatalytic performance. The anatase form of TiO_2 is preferable over rutile since anatase is found to be highly active in the photo-oxidation of organics when oxygen is used as an acceptor of photogenerated electrons [7].

X-ray diffraction scans (Fig. 4) provide evidence that anatase is the primary crystalline phase that develops in the thin films. By changing the level of atomic nitrogen doping (resulting from different N_2 flows, so a different N_2:O_2 reactive mixture ratio is achieved) during the sputtering process, there is a slight decrease in the anatase phase and increase in the development of the TiO_xN_y phase. By increasing the sputtering pressure, the

anatase peaks, especially **(101)** and **(004)**, located at $2\theta = 25.4°$ and $2\theta = 38.0°$ respectively, become less intense and broader. This indicates that the crystal size and the refractive index are decreasing [54]. At the same time, the **(103)**, **(112)**, and **(105)** orientations of the anatase crystal, located at $2\theta = 37.1°$, $38.7°$ and $54.1°$ respectively, disappeared as the higher pressure depositions were used. The **(105)** anatase peak was increased by increasing the nitrogen incorporation in the lattice. It is not surprising that the anatase **(101)** decreases rapidly by increasing the nitrogen flow rate. Many authors reported a crystal modification when substituting nitrogen into the anatase TiO_2 crystal. The wide peak between $2\theta = 41°$ and $44°$ is attributed to the presence of the TiO_xN_y phase accompanied with TiN_x and/or TiO_{55}. By changing the nitrogen flow rate, we can identify a remarkable formation of TiN crystals accompanied with oxygen vacancies in the lattice for nitrogen flow rates between **0.07** and **0.11** sccm, and it is more distinguishable at a higher sputtering pressure. Oxygen is a much more reactive element than nitrogen [45] so altering the oxygen to nitrogen flow rate's ratio can put considerable strains on the TiN crystallization process, explaining the observed broad diffraction peak at higher oxygen concentrations.
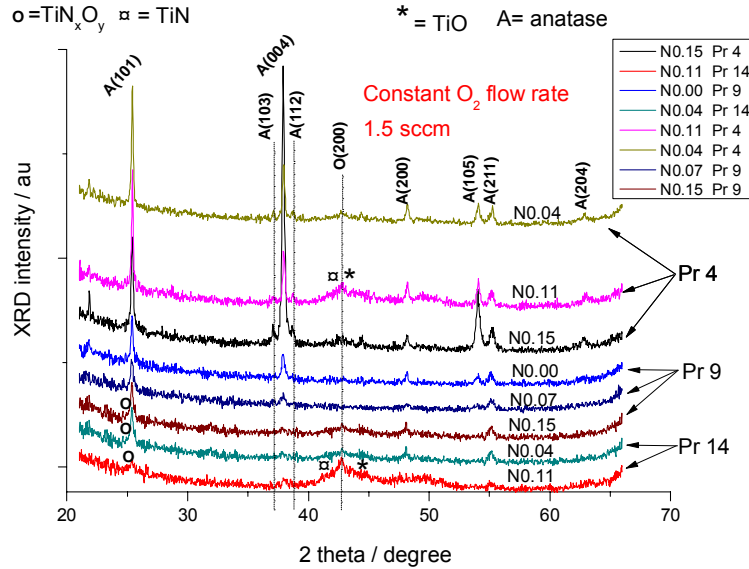

Fig. 4 – *XRD data obtained from TiO_2 films prepared at different pressures (Pr) and different Nitrogen flow rates (0.04 to 0.15 sccm)*

The avereage crystal size in each film was calculated from the anatase **(101)** peak using the Scherrer formula,

$$d = K\lambda/(\beta\cos\theta) \qquad (2)$$

where d is the crystal size in nm, K is a constant, λ is the XRD wavelength (in our case 1.54 Å), β is the full width at half maximum (FWHM), and θ is the diffraction angle. To try and understand the competitive nature of

nitrogen incorporation and the sputtering pressure, we plotted the surface response of the crystal size versus both variables (Fig. 5). It is apparent that the crystal size decreases by increasing the nitrogen flow rate, especially at higher pressure. However, this variation is less remarkable when working at low pressure (less than 9 mTorr).
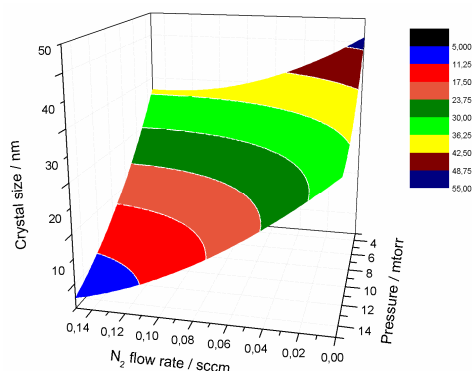
Fig. 5 − *Surface response of the crystal size versus deposition pressure and nitrogen flow rate*
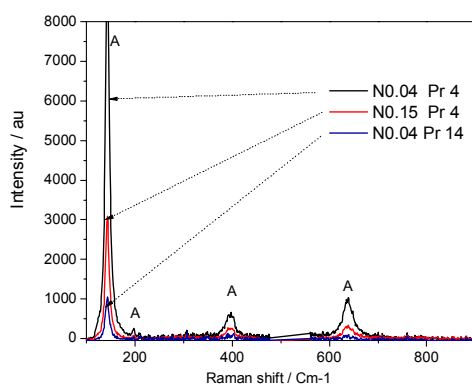
Fig. 5 − *Raman spectra of a selection of deposited films on silicon wafer*

The Raman shift spectra of the different thin films were measured and are shown in Fig. 6. All the samples show the typical Raman shift spectra of anatase TiO_2 [56-57], comprised of the peaks at 144 cm^{-1} (E_g, O−Ti−O bending mode), 198 cm^{-1} (B_{1g}/A_{1g}), 398 cm^{-1} (B_{1g}), and 640 cm^{-1} (E_g, Ti−O bond stretching mode). In addition to the optical band modes found by this method, no phonon line shifts were observed . Raman spectroscopic analysis can provide important information on the Ti−O bond lengths of the N-doped TiO_2 crystals from the stretching wave numbers which is related to the force constants and lengths of the bonding [2, 35]. There is no red shift in the E_g peak (at 640 cm^{-1} corresponding to the stretching vibrational mode of the Ti−O bond) when comparing the pure TiO_2 sample to any of the doped samples. The absence of the red shifting peak means that nitrogen is only substitutionally doped, and not found interstitially.
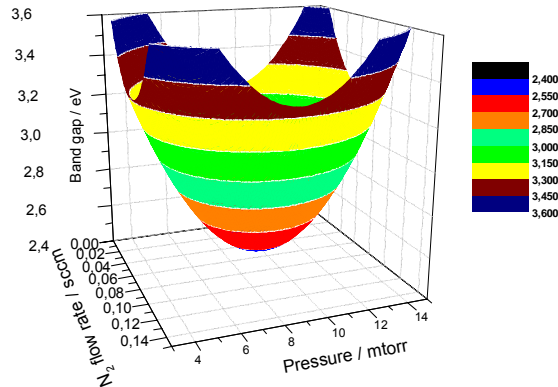
3.4   Band gap calculation

The optical properties of all samples were studied by measuring the transmission spectra in the UV-Visible range (210 to 1010 nm). The band gap values were calculated by the Tauc's equation using an indirect allowed transitions ($m = 2$),

$$\alpha h\nu = B(h\nu - E_g)^m, \qquad (3)$$

where α is the absorption coefficient, B is a constant called the edge width parameter, αh is the photon energy, E_g is the optical band gap, and m is a constant which is determined by the optical transition, either direct ($m = S$) or indirect ($m = 2$). The optical band gap is obtained from the extrapolation of the linear plots of $(\alpha h\nu)^{1/2}$ vs $h\nu$, where the x-intercept is the band gap energy. The calculated band gap values were estimated to be between 2.5 and 3.42 eV for the N-doped TiO_2 samples. This large difference is due to the different nitrogen concentrations and nitrogen positions in the lattice depending on the deposition pressure and the morphology of the various thin films. Oxygen vacancies can also have an important role on the band gap red shift.

The RSM of the modulated band gap (from the calculated ones) is presented in Fig. 7. It is clear that the conditions corresponding to the minimum band gap are in the same interval that display higher hydrophilicity. This is a very interesting correlation, suggesting that the position of the doped nitrogen energy levels within the band gap can have a substantial effect on the surface states of the material, which in turn affect its wettability.

Fig. 7 – *Modelling of the band gap calculated from the UV-Vis absorption spectra of glass coated by N doped TiO$_2$*

3.5 NMP degradation and optimization of the sputtering process

Using colored dyes as indicators in photocatalytic reactions can be difficult because it is sometime hard to separate the observed activity between the dye's photocatalytic decomposition, and the reduction of the dye due to the electron transfer reactions. In both cases we would get the dye's decoloration as that found with methylene blue [60]. We selected NMP because it is a pollutant in industrial waste water, and its concentration can be easily controlled by HPLC, which allows the observation of sub-components in real

time. Fig. 8 shows the NMP degradation with and without the presence of different thin films photocatalysts under UV irradiation. It is important to note that the pure TiO_2 has an intermediate effect compared to the other doped samples. This means that in some sputtering conditions, N-doped TiO_2 can enhance the photocatalytic activity under UV irradiation compared to pure TiO_2, while other sputtering conditions can have a negative effect on the photocatalytic reactions under UV illumination. This can reasonably explain the contradictions found in literature about the efficiency of nitrogen doping under UV illumination (see introduction).

The interaction of the plasma pressure and the nitrogen doping with respect to the photocatalytic decay of NMP in the TiO_2 thin films is shown in Fig. 9. We can distinguish two directions for the minimum NMP degradation time (optimum conditions). First, at higher pressure and lower nitrogen incorporation, porous thinner films are deposited with high active surface sites and show good efficiency for the photocatalysis in UV irradiation. On the other hand, a lower deposition pressure and higher nitrogen doping gives thicker films with less surface active sites, but still shows good photocatalytic activity. At an intermediate nitrogen doping and sputtering pressure, the deposition mechanism is more complicated.
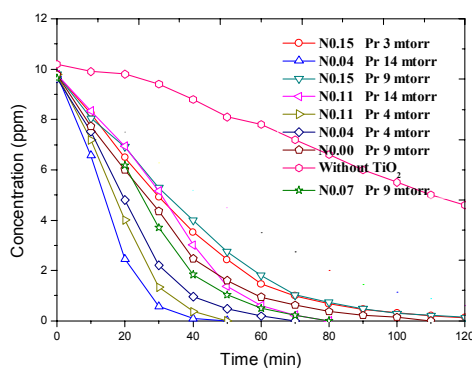

Fig. 8 − *NMP degradation time with different deposited TiO_2 samples*
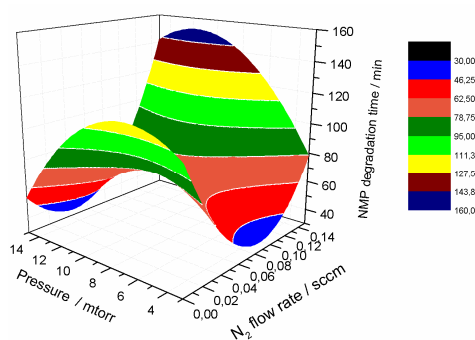

Fig. 9 − *Modelisation of NMP degradation time using the measured time up to total degradation by different samples*

It is well known that TiN and oxygen vacancies can increase the conductivity, and can also act as recombination centers in TiO_2 [61, 62]. At an

intermediate nitrogen flow rate, we found a remarkable formation of TiN crystals in the lattice, as shown in the XRD pattern in Fig. 4. This can explain the decreased photocatalytic efficiency at this interval of nitrogen flow rates (0.07 to 0.11 sccm), as TiN is not a good photocatalyst because it does not have semiconductor electronic properties, or good absorption in the UV range.

4. CONCLUSION

The efficiency of N doping in TiO_2 thin films to improve photocatalytic performance under UV irradiation may have a contradictory effect, which is clear from the literature survey. Using RF reactive sputtering as a deposition technique, we achieved different structures of N-doped TiO_2 (TiO_xN_y). There is a competitive effect of the morphology and the chemical composition on the efficiency of the photocatalytic activity under UV irradiation, which can be seen clearly using the response surface methodology, based on a design of experiment. The variation of surface wettability of the films over time in the dark is due to the hydrocarbon's adsorption on the surface of the TiO_2 thin films. Samples prepared at high pressure can have an optimized photocatalytic activity, even with lower film thicknesses, due to the high specific surface area and the optimal presence of TiO_xN_y crystals in the lattice. This study has shown that there is a delicate balance between the concentration and nature of nitrogen doping in TiO_2 that can lead to both improved and deteriorated photocatalytic activity. However, we have shown that there are optimal deposition conditions to maximize the photocatalytic efficiency of N-doped TiO_2, which can serve as a solid background for further investigations.

REFERENCE

1. U.G. Akpan, B.H. Hameed, *J. Hazard. Mater.* **170,** 520 (2009).
2. M. Kitano, M. Matsuoka, M. Ueshima, M. Anpo, *Appl. Catal. A: Gen.* **325,** 1 (2007).
3. F. Han, V.S. Rao Kambala, M. Srinivasan, *Appl. Catal. A: Gen.* **359,** 25 (2009).
4. I.N. Martyanov, K.J. Klabunde, *J. Catal.* **225,** 408 (2004).
5. H. Szymanowski, A. Sobczyk-Guzenda, A. Rylski, W. Jakubowski, M. Gazicki-Lipman, U. Herbert , F. Olcaytug, *Thin Solid Films,* **515,** 5275 (2007).
6. E. Aubry, M.N. Ghazzal, V. Demange, N. Chaoui, D. Robert, A. Billard, *Surf. Coat. Tech.* **201,** 7706 (2007).
7. A. Fujishima, X. Zhang, D.A. Tryk, *Surf. Sci. Rep.* **63,** 515 (2008).
8. B. Elvers, S. Hawkins, W. Russey, G. Schulz, *Encyclopedia of industrial chemistry* (VCH: New York: 1993).
9. D. Kaczmarek, D. Wojcieszak, J. Domaradzki, E. Prociow, *J. Phys.: Conf. Ser.* **146,** 012019 (2009).
10. Z. Liu, Y. Zhou, Z. Li, Yichao Wang, C. Ge, *J. Univ. Sci. Technol. B* **14,** 552 (2007).
11. Y. Li, M. Ma, X. Wang, Z. Li, *Surf. Coat. Tech.* **204,** 1353 (2010).
12. I.M. Arabatzis, T. Stergiopoulosa, M.C. Bernardc, D. Laboud, S.G. Neophytidesd, P. Falaras *Appl. Catal. B: Env.* **42,** 187 (2003).
13. T.C. Kaspar, T. Droubay, V. Shutthanandan, S.M. Heald, C.M. Wang, D.E. McCready, S. Thevuthasan, *Phys. Rev. B* **73,** 155327 (2006).
14. T. Yamaki, T. Sumita, S. Yamamoto, *J. Mater. Sci. Lett.* **21,** 33 (2002).

15. S.U.M Khan, M. Al-Shahry, W.B. Ingler, *Science* **297,** 2243 (2002).
16. A.V. Emeline, V.N. Kuznetsov, V.K. Rybchuk, N. Serpone, *Int. J. Photoenergy,* 258394 (2008).
17. K. Obata, H. Irie, K. Hashimoto, *Chem. Phys.* **339,** 124 (2007).
18. W. Smith, Y.P. Zhao, *J. Phys. Chem. C* 112, 19635 (2008).
19. C. Hu, X. Hu, L. Wang, J. Qu, A. Wang, *Environ. Sci. Technol.* **40,** 7903 (2006).
20. P.V. Kamat, *Chem. Rev.* **93,** 267 (1993).
21. I. Nakamura, N. Negishi, S. Kutsuna, T. Ihara, S. Sugihara, K. Takeuchi, *J. Mol. Catal. A: Chem.* **161,** 205 (2000).
22. P. Zeman, S. Takabayashi, *Surf. Coat. Tech.* **153,** 93 (2002).
23. T. Ihara, M. Miyoshi, Y. Iriyama, O. Matsumoto and S. Sugihara, *Appl. Catal. B: Env.* **42,** 403 (2003).
24. Y. Liu , X. Chen, J. Li, C. Burda, *Chemosphere* **61,** 11 (2005).
25. E. Borgarello, J. Kiwi, M. Gratzel, M. Pelizzetti, M. Visca, *J. Am. Chem. Soc.* **104,** 2996 (1982).
26. L. Spanhel, H. Weller, A. Henglein, *J. Am. Chem. Soc.* **109,** 3183 (1987).
27. R. Asahi, T. Morikawa, T. Ohwaki, K. Aoki, Y. Taga, *Science* **293,** 269 (2001).
28. T.L. Thompson, J.T. Yates, *Chem. Rev.* **106,** 4428 (2006).
29. W. Smith, S. Mao, G. Lu, A. Catlett, J. Chen, Y. Zhao, *Chem. Phys. Lett.* **485,** 171 (2010).
30. T. Morikawa, R. Asahi, T. Ohwaki, K. Aoki, K. Suzuki, Y. Taga, *R&D Review of Toyota CRDL,* **40** No.3 45 (2005).
31. T. Umebayashi, T. Yamaki, H. Itoh, K. Asai, *Appl. Phys. Lett.,* **81,** 454 (2002).
32. C. Di Valentin, E. Finazzi, G. Pacchioni, A. Selloni, S. Livraghi, M.C. Paganini, E. Giamello, *Chem. Phys.* **339,** 44 (2007).
33. D.J. Mowbray, J.I. Martinez, J.M. Garcia Lastra, K.S. Thygesen, K.W. Jacobsen *J. Phys. Chem. C* **113,** 12301 (2009).
34. J. Wang, D.N. Tafen, J.P. Lewis, Z. Hong, A. Manivannan, M. Zhi, M. Li, N. Wu, *J. Am. Chem. Soc.* **131,** 12290 (2009).
35. S. Lee, I. Cho, D.K. Lee, D.W. Kim, T.H. Noh, C.H. Kwak, S. Park, K.S. Honga, J.K. Lee, H.S. Jung, *J. Photoch. Photobio. A* **213,** 129 (2010).
36. S.H. Lee, E. Yamasue, K.N. Ishihara, H. Okumura, *Appl. Catal. B: Env.* **93,** 217 (2010).
37. O. Diwald, T.L. Thompson, T. Zubkov, E.G. Goralski, S.D. Walck, J.T. Yates, *J. Phys. Chem. B* **108,** 6004 (2004).
38. O. Diwald, T.L. Thompson, E.G. Goralski, S.D. Walck, J.T. Yates, *J. Phys. Chem. B* **108,** 52 (2004).
39. F. Dong,W. Zhao, Z. Wu, S. Guo, *J. Hazard. Mater.* **162,** 763 (2009).
40. A. Brudnik, M. Bucko, M. Radecka, A. Trenczek-Zajac, K. Zakrzewska, *Vacuum* **82,** 936 (2008).
41. U. Helmersson, M. Lattemann, J. Bohlmark, A.P. Ehiasarian, J.T. Gudmundsson, *Thin Solid Films* **513,** 1 (2006).
42. W.D. Sproul, D.J. Christie, D.C. Carter, *Thin Solid Films* **491,** 1 (2005).
43. F. Perry, A. Billard, C. Frantz, *Surf. Coat. Tech.* **94-95,** 681 (1997).
44. J.W. Bradley, T. Welzel, (Process Diagnostics), S. Konstantinidis, F. Gaboriau, M. Gaillard, M. Hecq, A. Ricard, (Optical Plasma Diagnostics During Reactive Magnetron Sputtering), *Reactive Sputter Deposition* (Springer Berlin Heidelberg New York: 2008).
45. A. Trenczek-Zajac, M. Radecka, K. Zakrzewska, A. Brudnik, E. Kusior, *J. Power Sources* **194,** 93 (2009).
46. J. Musil, P. Baroch, J. Vlcek, K.H. Nam, J.G. Han, *Thin Solid Films* **475,** 208 (2005).
47. B.C. Trasferetti, C.U. Davanzo, R.A. Zoppi, *Phys. Rev. B* **64,** 125404 (2001).
48. M.S. Wong , H.P. Chou, T.S. Yang, *Thin Solid Films* **494,** 244 (2006).

49. W. Zhou, X. Zhong, X. Wu, L. Yuan, Q. Shu,W. Li, Y. Xia, *J. Phys. D: Appl Phys.* **40,** 219 (2007).
50. C. Wang, H. Groenzin, M.J. Shultz, Langmuir **19,** 7330 (2003).
51. S.L.C. Ferreira, W.N.L. dos Santos, C.M. Quintella, B.B. Neto, J.M. Bosque-Sendra, *Talanta* **63,** 1061 (2004).
52. M.A. Bezerra, R.E. Santelli, E.P. Oliveira, L.S. Villar, L.A. Escaleira, *Talanta* **76,** 965 (2008).
53. X.T. Zhao, K. Sakka, N. Kihara, Y. Takada, M. Arita, M. Masuda, *Microelectr. J.* **36,** 549 (2005).
54. K. Eufinger, D. Poelman, H. Poelman, R. De Gryse, G.B. Marin, *J. Phys. D: Appl. Phys.* **40,** 5232 (2007).
55. N. Martin, R. Sanjines, J. Takadoum, F. Levy, *Surf. Coat. Tech.* **142-144,** 615 (2001).
56. M. Ritala, M. Leskela Erja Nykдnen, P. Soininen, L. Niinisto, *Thin Solid Films* **225,** 288 (1993).
57. W.R. Kaiser, A.N. Christensen, G. Mullervogt, *Phys. Rev. B,* **17** 1095 (1978).
58. L. Popovic, D. de Waal, J.C.A. Boeyens, *J. Raman Spectrosc.* **36,** 2 (2005).
59. T. Ohsaka, F. Izumi, Y. Fujiki, *J. Raman Spectrosc.* **7,** 321 (1978).
60. A. Mills, J. Wang, *J. Photoch. Photobio. A* **127,** 123 (1999).
61. H.M. Yates, M.G. Nolana, D.W. Sheela, M.E. Pemble, *J. Photoch. Photobio. A* **179,** 213 (2006).
62. S. Takeda, S. Suzuki, H. Odaka, H. Hosono, *Thin Solid Films* **392,** 338 (2001).